

# Structural changes in the calcium pump accompanying the dissociation of calcium

Chikashi Toyoshima & Hiromi Nomura

*Institute of Molecular and Cellular Biosciences, The University of Tokyo, Bunkyo-ku, Tokyo 113-0032, Japan*

**In skeletal muscle, calcium ions are transported (pumped) against a concentration gradient from the cytoplasm into the sarcoplasmic reticulum, an intracellular organelle. This causes muscle cells to relax after cytosolic calcium increases during excitation. The  $\text{Ca}^{2+}$  ATPase that carries out this pumping is a representative P-type ion-transporting ATPase. Here we describe the structure of this ion pump at 3.1 Å resolution in a  $\text{Ca}^{2+}$ -free (E2) state, and compare it with that determined previously for the  $\text{Ca}^{2+}$ -bound (E1 $\text{Ca}^{2+}$ ) state. The structure of the enzyme stabilized by thapsigargin, a potent inhibitor, shows large conformation differences from that in E1 $\text{Ca}^{2+}$ . Three cytoplasmic domains gather to form a single headpiece, and six of the ten transmembrane helices exhibit large-scale rearrangements. These rearrangements ensure the release of calcium ions into the lumen of sarcoplasmic reticulum and, on the cytoplasmic side, create a pathway for entry of new calcium ions.**

P-type ion transporting ATPases, which include  $\text{Na}^+\text{K}^+$ -ATPase and gastric  $\text{H}^+\text{K}^+$ -ATPase among others, are fundamental in establishing ion gradients by pumping ions across biological membranes (reviewed in ref. 1). Of many P-type ATPases known today,  $\text{Ca}^{2+}$ -ATPase (SERCA1a) from skeletal muscle sarcoplasmic reticulum (SR) is structurally and functionally the best-studied member<sup>1–3</sup>. SR  $\text{Ca}^{2+}$ -ATPase pumps  $\text{Ca}^{2+}$  from the cytoplasm into the reticulum, thereby causing the relaxation of muscle cells. Two  $\text{Ca}^{2+}$  ions can be transported per ATP hydrolysed and two or three  $\text{H}^+$  ions are counter-transported<sup>4</sup>.

Active transport of  $\text{Ca}^{2+}$ -ATPase is achieved, according to the E1–E2 model<sup>5,6</sup>, by changing the affinity of  $\text{Ca}^{2+}$ -binding sites from high (E1) to low (E2)<sup>7</sup>. The release of  $\text{Ca}^{2+}$  ‘occluded’ in the transmembrane binding sites takes place during the transition from E1P to E2P (‘P’ indicating that the enzyme is phosphorylated; Fig. 1, inset). Autophosphorylation of an aspartyl residue in the reaction cycle is a characteristic feature of the P-type ATPases. However, the residues constituting the phosphorylation site are shared by the members in the haloacid dehalogenase superfamily<sup>8</sup> and by many bacterial response regulators, despite the differences in the folding patterns (reviewed in ref. 9).

We previously determined the structure of SR  $\text{Ca}^{2+}$ -ATPase<sup>10</sup> with two bound  $\text{Ca}^{2+}$  in the transmembrane (M) region, which consists of ten  $\alpha$ -helices (Fig. 1; Protein Data Bank, PDB, code 1EUL). The cytoplasmic part of  $\text{Ca}^{2+}$ -ATPase consists of three domains (A, actuator or anchor; N, nucleotide; and P, phosphorylation), well separated in this  $\text{Ca}^{2+}$ -bound (E1 $\text{Ca}^{2+}$ ) form. The phosphorylation residue, Asp 351, is located on the P domain, and the adenosine moiety of ATP binds to the N domain. Modelling the structures (PDB codes 1FQU (ref. 10) and 1KJU (ref. 11)) based on low-resolution maps of the tubular crystals<sup>11,12</sup>, in which the enzyme is in a state similar to E2P (ref. 13), showed large movements of the three cytoplasmic domains to form a compact headpiece. These rearrangements of the cytoplasmic domains must be associated with the changes in the transmembrane binding sites<sup>14</sup>, but the molecular mechanism was far beyond what we could imagine.

Here we describe the crystal structure of  $\text{Ca}^{2+}$ -ATPase in the absence of  $\text{Ca}^{2+}$  and in the presence of thapsigargin, a potent inhibitor that fixes the enzyme in a form analogous to E2 (ref. 15), abbreviated as E2(TG). The structure (Figs 1 and 2), deter-

mined to 3.1 Å resolution, is very different from that of E1 $\text{Ca}^{2+}$ , yet can be compared directly, because no ATP or phosphorylation is involved in the transition between them. The movements of cytoplasmic domains are even larger than we described for the tubular crystals<sup>10</sup>. Transmembrane helices undergo drastic rearrangements that involve shifts normal to the membrane. These movements have clear mechanistic implication in the release and binding of  $\text{Ca}^{2+}$ . Knowing the second structure in the reaction cycle, we can now begin to understand how ion pumps work.

## Structure determination

The crystals of SR  $\text{Ca}^{2+}$ -ATPase were grown by dialysis in the presence of thapsigargin and exogenous lipid. Thapsigargin was added before the addition of EGTA for removing  $\text{Ca}^{2+}$ . Two types of crystals of different symmetry ( $P2_1$  and  $P4_1$ ) appeared but only those belonging to the space group  $P4_1$  diffracted to 3.1 Å resolution at the BL44XU beam line of SPring-8. The structure was solved by molecular replacement and refined to an  $R_{\text{free}}$  of 26.8%. Inclusion of  $\text{Ca}^{2+}$  (1 mM) in the dialysis buffer did not affect the crystal quality or bring differences in the final model. The structure of  $\text{Ca}^{2+}$ -ATPase in E2(TG) form, in comparison with E1 $\text{Ca}^{2+}$ , is shown in Figs 1 and 2. We describe the structural changes as those accompanying the transition from E1 $\text{Ca}^{2+}$  to E2(TG), mainly because we prepared the crystals by removing  $\text{Ca}^{2+}$ .

## Movements of the cytoplasmic domains

To realize the close association of the three cytoplasmic domains widely separated in E1 $\text{Ca}^{2+}$ , the N domain inclines nearly 90° with respect to the membrane (Fig. 2a) and the A domain rotates by about 110° horizontally (Fig. 2b; Supplementary Information Animation 3). As a result, the top part of the N domain moves more than 50 Å. Also, the trypsin digestion site on the A domain (T2 in Fig. 1), which is well exposed in E1 $\text{Ca}^{2+}$ , is partially blocked by the P domain<sup>13</sup> (Supplementary Information Animation 3). The cytoplasmic domains move as a whole in an M10-to-M1 direction (~23 Å for the P domain).

Two components contribute to this large change in inclination of the N domain: the first is the movement of the P domain (see, for example, the change in inclination of the P5 helix in Fig. 2a), and the other is that of the N domain itself relative to the P domain. An

analysis by Dyndom<sup>16</sup> indicates that the P domain inclines by about 30° with respect to the membrane, and the N domain by about 50° relative to the P domain. This 30° inclination of the P domain is directly related to tilting of the transmembrane helices, in particular the M5 helix, and is likely to be a central event in the active transport (see below).

Despite the large movements between the two states, the structure of the P and N domains remain virtually the same (r.m.s. deviations 0.63 and 0.75 Å, respectively; Fig. 3 and Supplementary Information Animation 3), except for a few 'hinge' residues and those at the A–P interface. The hinge region (DPPR starting from Asp 601 and TNQMS starting from Thr 358) is well hydrogen bonded between the two strands; no hydrogen bonds favouring E2(TG) can be identified, although it is generally difficult to assign hydrogen bonds at 3.1 Å resolution. This suggests that stabilization of the closed configuration takes place entirely at the A–N and A–P interfaces, where we can identify a few hydrogen bonds (Fig. 1). The residues at the A–P interface (Ile 179–Thr 181 in A, and Asp 703–Asn 706 in P) contain signature sequences of the P-type ATPases (reviewed by ref. 1).

**Rearrangement of transmembrane helices**

The dissociation (or binding) of Ca<sup>2+</sup> accompanies dramatic rearrangements of six (M1–M6) out of ten transmembrane helices (Figs 2 and 4a). The rearrangements are not limited to those constituting the Ca<sup>2+</sup>-binding sites (M4–M6, M8) and appear quite complicated: M1 and M2 move upwards (+z direction, towards the cytoplasm) whereas M3 and M4 shift downwards,

both up to about 5 Å, close to one turn of an α-helix (5.4 Å; Figs 1 and 2). M1 shows a large lateral movement within the membrane (Fig. 2b), and is unique in this respect. M3 and M5 are strongly curved in E2(TG) but in opposite directions (Figs 1 and 2). Our first goal is, therefore, to understand how these complicated movements are organized and linked with those of the cytoplasmic domains. We can start with the many places where a movement of one helix could cause the movements of others (a 'domino' effect). For example, in Fig. 4a, inclination of M4 must impinge on M2 at the top, causing M2 itself to tilt. It also helps to note that the movements of helices normal to the membrane are in most cases produced by the changes in their inclinations (for example, M2). However, it seems most critical to understand the links between the transmembrane helices and the P domain.

M5 runs through the centre of the enzyme from the luminal surface to the end of the P domain, where it is integrated as a part of the Rossmann fold (Fig. 3). Hence, the top part of M5 moves together with the P domain as a single entity. In fact, if the two structures are superimposed with the P domain, the top part of M5 also superimposes virtually completely (Fig. 3). Here, short anti-parallel β-strands (0 and 7) of the P domain appear to 'clamp' the M4 and M5 helices (Fig. 3). The middle part of M5 is linked to the loop (L67) connecting M6 and M7 (through Arg 751; Fig. 1), perhaps restricting the bowing of M5; this loop is also hydrogen bonded to the P domain (refer to Fig. 8 of ref. 10) and is important in phosphorylation<sup>17</sup>. On the opposite side of the P domain to M4, M3 is located. The top part of M3 is connected to the P1 helix at the bottom of the P domain through a critical hydrogen bond<sup>18</sup>

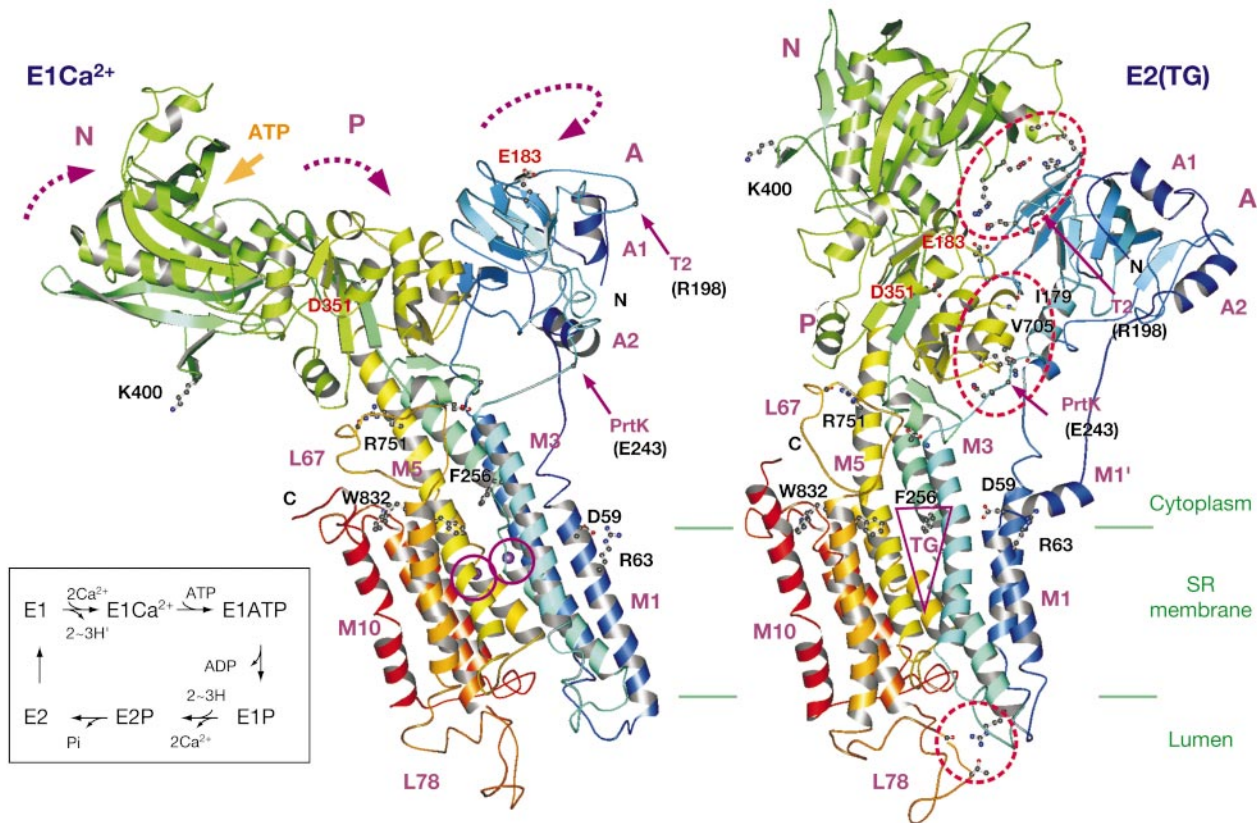


**Figure 1** Ribbon representation of SR Ca<sup>2+</sup>-ATPase in the Ca<sup>2+</sup>-bound form (E1Ca<sup>2+</sup>) and that (E2(TG)) in the absence of Ca<sup>2+</sup> but in the presence of thapsigargin (TG). Inset, a simplified reaction scheme (showing only the forward direction). Colours change gradually from the amino terminus (blue) to the carboxy terminus (red). Two purple spheres (circled) in E1Ca<sup>2+</sup> represent bound Ca<sup>2+</sup>. Red circles in E2(TG) indicate extra hydrogen bonds in E2(TG). Large arrows in E1Ca<sup>2+</sup> indicate the direction of movement of the cytoplasmic

domains during the change from E1Ca<sup>2+</sup> to E2(TG). PtrK, proteinase-K digestion site (around Glu 243; ref. 27); T2, trypsin digestion site at Arg 198 (ref. 41); ATP, binding pocket for the adenosine moiety of ATP. Principal residues are marked: E183 (A domain), F256 (thapsigargin-binding site), D351 (P domain, phosphorylation site), K400 (N domain, phospholamban-binding site<sup>42</sup>) and R751 (linking M5 and the loop (L67) connecting M6 and M7). Prepared with Molscript<sup>43</sup>.



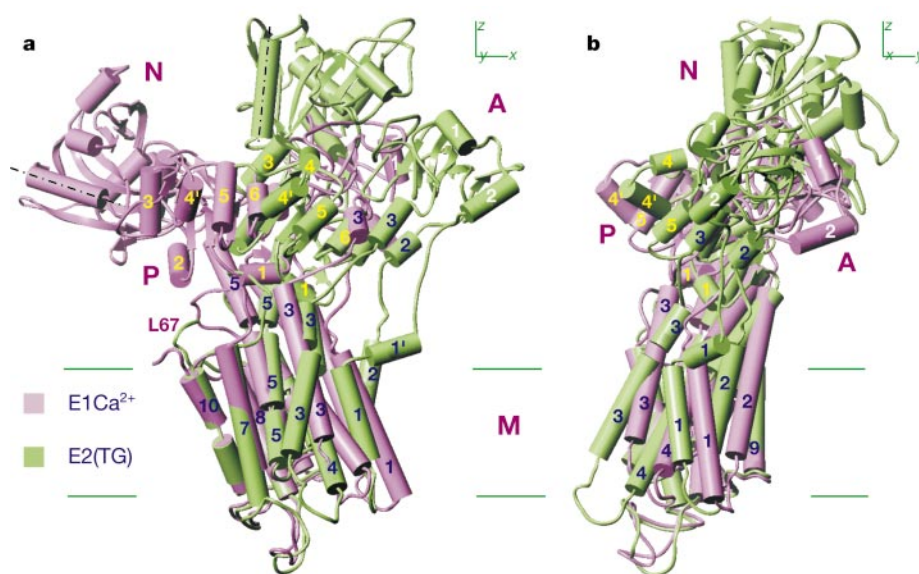


**Figure 2** Superimposition of the  $\text{Ca}^{2+}$ -bound form ( $\text{E1Ca}^{2+}$ , violet) and the thapsigargin-bound form ( $\text{E2(TG)}$ , light green) of  $\text{Ca}^{2+}$ -ATPase fitted with the transmembrane domain.  $\alpha$ -Helices are represented by cylinders and  $\beta$ -strands by arrows. Both are viewed along the membrane plane, but from nearly orthogonal directions (specified in the top right

corners). M5 is represented with three cylinders, and M3 with two cylinders, although they are continuous helices. Dash-dotted lines in **a** show the orientations of a helix in the N domain in the two states. Also see Supplementary Information Animations 1 and 2.

involving Glu 340 (Fig. 3).

Thus, M3–M5 helices are directly linked to the P domain by hydrogen bonds. M6 is also connected, although less directly, to the P domain through L67 (Fig. 4a) and M5 (by hydrogen bonds between Asn 756 and the carbonyl of Gly 808 and Asn 810). If the P domain inclines, for instance, owing to the bending of M5, all of these helices (M3–M6) will incline and generate movements that have components normal to the membrane. Their amounts depend on the distances from the pivoting point (Fig. 4b), which is located around Gly 770 (on M5), a critical residue<sup>19</sup>, at the middle of the membrane (double circle on M5 in Fig. 4a). There, M5 is tightly packed against M7 with a cluster of four (one on M5, three on M7) glycines, and the lower part below Gly 770 hardly moves (Fig. 4a;

Supplementary Information Animation 4). The shift is therefore small for M6 and large for M3 and M4 (Figs 2 and 4a); whole M3 and M4 helices move downwards during dissociation of  $\text{Ca}^{2+}$ , whereas M6 undergoes more-local changes (Supplementary Information Fig. 1).

Because tilting of the P domain will cause different movements in different parts of the protein, interfaces between them will change. This might result in steric clashes, which can be avoided only by adjusted movements. For instance, if the M3 helix moved as a single entity with the P domain, the luminal end would collide with M5 (Fig. 2a). The large  $-y$  component of the movement of M3 (Fig. 2b) must be to avoid this (or is guided by the steric constraints). The movement of M4 is also explained in this way. To be able to change the interface between transmembrane helices, hydrogen bonds between them should be avoided, which is certainly the case. The ‘joints’ also need to be flexible. In fact, M3–M5 helices do not actually move with the P domain as a single entity. Only the top part of M5 does so; M4 differs in orientation even at the top (Fig. 3). Presumably this is because the  $\beta$ -strands clamping M5 and M4 (0 and 7; Fig. 3) are short and located at an end of the  $\beta$ -sheet in the Rossmann fold, allowing more freedom. The link between the P domain and M3 involves the long side chain of Glu 340 (Fig. 3). Thus, the P domain, with flexible joints, functions as a coordinator of the transmembrane helices that gather by mostly van der Waals interactions.

It is now easy to see that the P domain will conduct the movements of M1 and M2, although they are not directly connected. M1 and M2 are characterized by their upward movements with  $\text{Ca}^{2+}$  dissociation. The movement of M1 is complex: the top part of M1 is largely bent at Asp 59 (Fig. 1) and forms an amphipathic helix having hydrophobic residues (Phe, Leu and Ile) on one side and charged residues (Glu 58, Asp 59) on the other (M1’ in Fig. 2). This bending may have occurred as a result of steric collision with M3, because M3 inclines and move downwards whereas M1 moves upwards. M2 is an inclined helix in  $\text{E1Ca}^{2+}$  but nearly upright in  $\text{E2(TG)}$  (Fig. 4a). This change in inclination, apparently caused by M4 (Fig. 4a), results in a large ( $\sim 5 \text{ \AA}$ ) upward movement near the cytoplasmic surface but hardly any at the luminal end. In contrast, M1 moves upwards without changing its inclination, but also moves

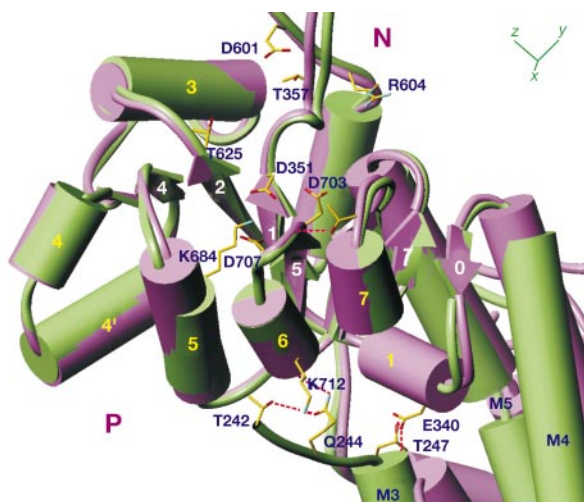


**Figure 3** Interface between the transmembrane helices (M3–M5) and the P domain of  $\text{Ca}^{2+}$ -ATPase. Superimposition of the  $\text{Ca}^{2+}$ -bound ( $\text{E1Ca}^{2+}$ , violet) and thapsigargin-bound ( $\text{E2(TG)}$ , light green) forms fitted with the P domain. The residues (in atom colour) represent those in  $\text{E2(TG)}$ . Links between the P1 and M3 helices involve hydrogen bonds between E340 and NH of L249 (not seen) as well as OH of T247 near the top of M3. Also see Supplementary Information Animation 3.

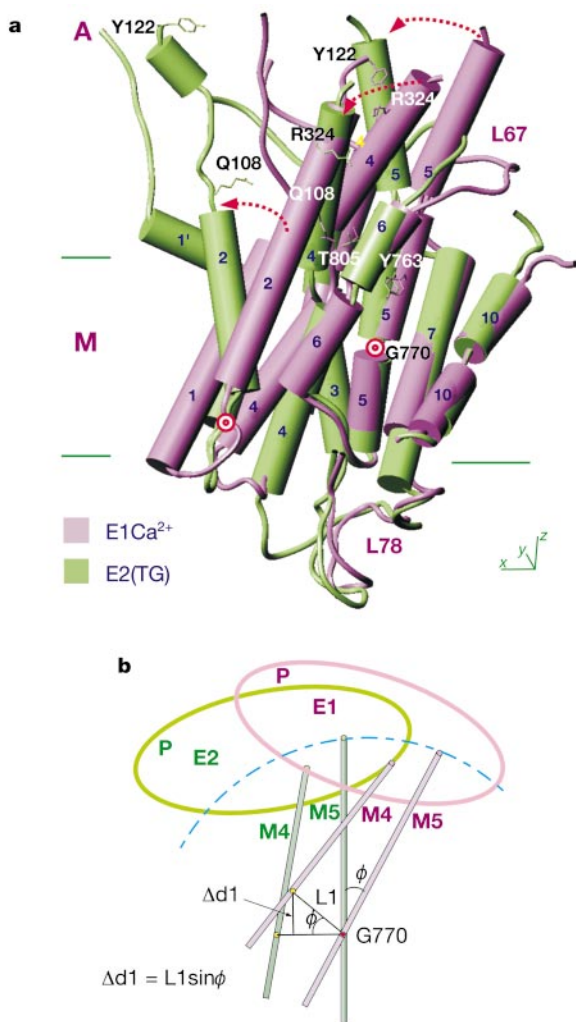


**Figure 4** Rearrangement of transmembrane helices viewed from the rear (**a**), and a diagram illustrating the shift of M4 normal to the membrane by the tilting of M5 (**b**). The models for E1Ca<sup>2+</sup> (violet) and E2(TG) (light green) are superimposed. The M5 helix lies along the plane of the paper. M8 and M9 are removed in **a**. Double circles show pivot positions for M2 and M5. Arrows indicate the directions of movements during the change from E1Ca<sup>2+</sup> to E2(TG). In **b**, M4 and M5 are linked in the P domain (ovals) and move as a rigid body. Tilting of M5 around the pivoting point (Gly 770) generates a vertical shift of  $\Delta d1$  for M4 without a large horizontal shift at the level of the pivoting point. For  $L1 = 10 \text{ \AA}$  and  $\phi = 30^\circ$ ,  $\Delta d1$  becomes  $5 \text{ \AA}$ . Also see Supplementary Information Animation 4.

horizontally (pushed by M2; Fig. 2b). The top part of M2 seems to be positioned by Tyr 122 with a hydrogen bond to Arg 324 (M4) in E1Ca<sup>2+</sup> (Fig. 4a). This will break with the inclination of M4. In E2(TG), M2 is partly unwound but the top part remains, packed against the P domain (Fig. 4a). Thus, although M1 and M2 are connected to the A domain and expected to be important in its rotation, their movements are likely to be governed by the P domain.

**Changes around the Ca<sup>2+</sup>-binding sites**

These movements of transmembrane helices have clear meanings in ion binding and dissociation. Figure 5 shows a more detailed view around the Ca<sup>2+</sup>-binding sites. The two sites (I and II) have different coordination geometry<sup>10</sup> and biochemical properties<sup>20</sup>. Site I, presumably the binding site for the first Ca<sup>2+</sup> ion<sup>20,21</sup>, entirely consists of side-chain oxygen atoms (Fig. 5a) of residues on three helices (M5, M6 and M8). Site II, with an arrangement of oxygen atoms reminiscent of the EF-hand motif<sup>22</sup>, is formed nearly ‘on’ the

M4 helix; three carbonyl oxygen atoms from residues on M4 contribute, and Glu 309 caps the bound Ca<sup>2+</sup> from above (Fig. 5a). To realize efficient coordination of Ca<sup>2+</sup>, both M4 and M6 helices have unwound parts (Supplementary Information Fig. 1).

In site I, we see marked changes with the residues on M6. Three crucial residues, Asn 796, Thr 799 and Asp 800, rotate nearly 90° clockwise (orange arrows in Fig. 5c) accompanying the dissociation of Ca<sup>2+</sup>. As a result, Thr 799 orients away from the molecule’s centre, and is replaced by Asp 800 (Fig. 5c). Asn 768 moves away towards site II. The backbone of Glu 771 and Glu 908 hardly move. In short, the change in inclination of M5 above Gly 770 (Fig. 4a) decreases the number of oxygen atoms that can contribute to site I. In site II, Glu 309 now points away from the binding site (Fig. 5b), M4 is shifted downwards, and Asp 800 moves away (Fig. 5c). The carbonyl groups involved in Ca<sup>2+</sup> binding may make hydrogen bonds with Asn 768 and Asn 796, both of which have moved closer to M4.

This configuration of M6 in E2(TG) seems to be stabilized by a hydrogen bond between Ser 940 (M9) and the main-chain carbonyl of Thr 799 (Fig. 5b), which was hydrogen bonded to the hydroxyl of Tyr 763 in E1Ca<sup>2+</sup>. The carbonyl oxygen of Asp 800, binding water in E1Ca<sup>2+</sup>, seems to make a hydrogen bond with the amide of Ala 804 (Supplementary Information Fig. 1). Ser 767 may work as the hydrogen bond donor for Glu 771 and Asp 800. At this resolution, however, hydrogen-bonding networks remain ambiguous, particularly because no water molecules can be identified.

These changes clearly explain the decrease of affinity for Ca<sup>2+</sup>, although it is unclear why such complicated movements are required. Homology modelling of the cation-binding sites of Na<sup>+</sup>K<sup>+</sup>-ATPase (H. Ogawa and C.T., unpublished data) provides a clue. With the arrangements of residues shown here, it was straightforward to make two high-affinity K<sup>+</sup>-binding sites, as long as Asn 796 is replaced by Asp, after the Na<sup>+</sup>K<sup>+</sup>-ATPase sequence: the other coordinating residues are common to both ATPases. The key feature in the model is that the Asp (Asn 796) is coordinated to both K<sup>+</sup>, similar to Asp 800 in coordination of two Ca<sup>2+</sup>. Because Asn 796 is located one turn below where Asp 800 was, M4 must move downwards to provide carbonyl groups for coordination of K<sup>+</sup>. It is well established that K<sup>+</sup> affects many kinetic parameters of Ca<sup>2+</sup>-ATPase, although in millimolar range (for example, ref. 23). We therefore suggest that large complicated movements are needed for counter-transport. It would be interesting to know what ions are counter-transported by the pump protein ancestral<sup>1</sup> to both Ca<sup>2+</sup>- and Na<sup>+</sup>K<sup>+</sup>-ATPases.

**Thapsigargin-binding site**

It was necessary to include thapsigargin in the specimen to keep the enzyme from denaturing in the absence of Ca<sup>2+</sup>. Thapsigargin has attracted considerable interest because of its high affinity (subnanomolar dissociation constant<sup>15</sup>) and specificity. Thapsigargin is a hydrophobic molecule that is thought to bind to the M3 helix around Phe 256 (refs 24, 25). Our study unambiguously identifies its binding site: the cavity surrounded by the M3, M5 and M7 helices near the cytoplasmic surface of the membrane (Fig. 6). Bulky hydrophobic residues on these three helices form a complementary surface to thapsigargin, which, with a potential hydrogen bond with Ile 829 (Fig. 6), effectively reduces the movements of transmembrane helices. In E1Ca<sup>2+</sup> this cavity is narrower (Fig. 2a) and the surface is not complementary because of the shift of M3.

Why thapsigargin can save solubilized Ca<sup>2+</sup>-ATPase from denaturation is worth considering. The instability suggests that thermal movements of transmembrane helices become deleteriously large when left without the support of lipids or the cohesion provided by bound Ca<sup>2+</sup>. In fact, phospholipids and millimolar Ca<sup>2+</sup> are necessary for long-term stability of this enzyme<sup>26</sup>. High Ca<sup>2+</sup> concentrations will work as a kind of inhibitor that limits the movement of transmembrane helices essential for Ca<sup>2+</sup> transport.



Requirement of millimolar  $\text{Ca}^{2+}$  has also been demonstrated by protection to the cytoplasmic domains against proteinase K attack<sup>27</sup>. In  $\text{Na}^+\text{K}^+$ - and  $\text{H}^+\text{K}^+$ -ATPases, transmembrane helices come out of the membrane after proteolysis and mild heat treatment<sup>28,29</sup>. This happens only in the absence of  $\text{K}^+$ . These results suggest that transmembrane helices undergo large-scale movements when binding cations are absent, and that the movements are linked with those of the cytoplasmic domains.

### Access pathway to the binding sites

In the classical E1–E2 models, E2 is described as having low-affinity  $\text{Ca}^{2+}$ -binding sites exposed to the lumen, and  $\text{Ca}^{2+}$  binding from the cytoplasmic side requires prior conversion to an E1 form<sup>7</sup>. Therefore we do not know whether we should expect to see, in the E2(TG) structure, an ion pathway to the transmembrane binding sites. Yet a water-accessible channel clearly exists that has an opening ( $8 \times 10 \text{ \AA}$ ) lined by negatively charged residues and leads to the carboxyl group of Glu 309 (Supplementary Information Fig. 2). It is therefore tempting to speculate that the first event in the  $\text{Ca}^{2+}$  binding is an interaction with Glu 309, followed by a conformation change of the side chain to deliver the  $\text{Ca}^{2+}$  to the binding cavity. Indeed, there is no room for  $\text{Ca}^{2+}$  to pass around Glu 309 to reach the binding sites. This channel disappears in  $\text{E1Ca}^{2+}$  owing to the movements of M1 and M3.

On the luminal side, the loop connecting M3 and M4 comes closer to the L78 loop (Fig. 2a), sealing the access pathway at the very surface. In  $\text{E1Ca}^{2+}$ , the pathway is much deeper, coming close to the  $\text{Ca}^{2+}$ -binding sites. Thus, in this aspect, the structure deviates from the classical E1–E2 models that assume lumenally opened binding

sites<sup>7</sup>. However, in the normal reaction cycle, the luminal gate is presumably opened during the E1P-to-E2P transition, and the counter ions ( $\text{H}^+$  in this case) bind then (Fig. 1, inset). Hence, in E2, because the counter ions have already bound, it will be more efficient for a pump to close the luminal gate and prepare for the entry of new  $\text{Ca}^{2+}$  from the cytoplasmic side. These features are exactly what we see in the structure presented here.

### Conclusion

As described,  $\text{Ca}^{2+}$ -ATPase seems to undergo, in the absence of  $\text{Ca}^{2+}$ , large-scale thermal movements involving both transmembrane and cytoplasmic domains, and the P domain is the coordinator of the movements. If so, we expect the SR vesicles with loaded  $\text{Ca}^{2+}$  to show significant leakage, and thapsigargin to stop it. This has indeed been demonstrated (G. Inesi, personal communication). Certainly, the closed configuration of the cytoplasmic domains will limit such movements and therefore the leakage. Another role of the closed configuration is to stop the reaction cycle, which is regulated essentially by  $\text{Ca}^{2+}$  alone. ATP can bind to the enzyme even when  $\text{Ca}^{2+}$  is absent but, without  $\text{Ca}^{2+}$ , the reaction cycle cannot proceed. In the closed configuration, the  $\gamma$ -phosphate of ATP comes close to, but cannot reach, the phosphorylation residue Asp 351. It requires deeper inclination of the N domain, or the rotation of the A domain to release the N domain. This in turn requires the binding of  $\text{Ca}^{2+}$ , which will fix the transmembrane helices in different positions and will prevent the tilting of the P domain to form a closed configuration. In this regard, it is noteworthy that the A-domain rotation takes place during the E1P-to-E2P transition<sup>14</sup>, and that the proteolytic cut of the link

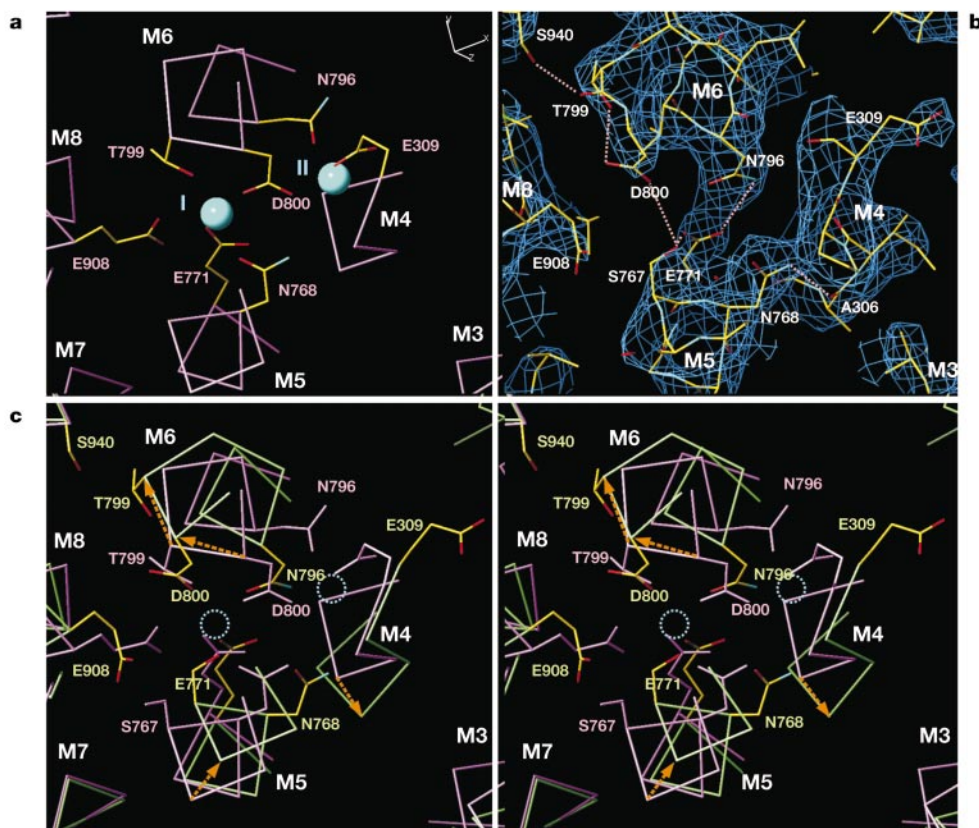


**Figure 5** Conformation changes around the  $\text{Ca}^{2+}$ -binding sites. **a**,  $\text{C}\alpha$  trace and the side chains of the coordinating residues in  $\text{E1Ca}^{2+}$ . **b**, Composite omit map<sup>37</sup> (at  $1.2\sigma$ ) and the model for the corresponding area in E2(TG). **c**, Stereo view of the composite of the models for  $\text{E1Ca}^{2+}$  (violet) and E2(TG) (atom colour). The viewing direction is approximately down

the M5 helix in  $\text{E1Ca}^{2+}$ . Two bound  $\text{Ca}^{2+}$  appear as cyan spheres (**a**) or circles (**c**). Dashed lines in **b** show potential hydrogen bonds. Orange arrows in **c** show the movements of the corresponding residues during the change from  $\text{E1Ca}^{2+}$  to E2(TG).

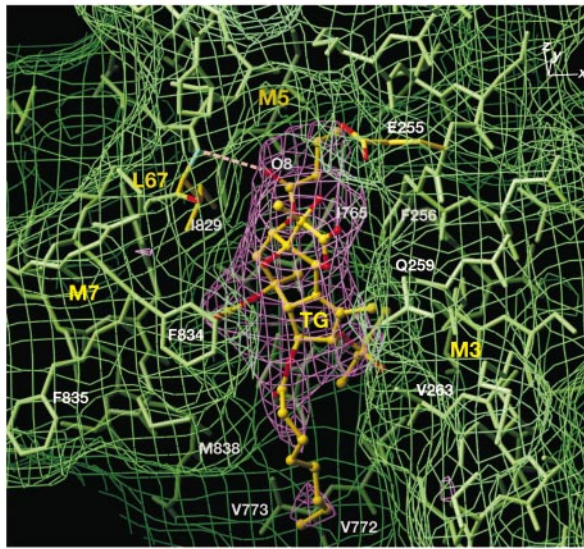


**Figure 6** Thapsigargin (TG) binding site in  $\text{Ca}^{2+}$ -ATPase. TG is in atom colour, and  $\text{Ca}^{2+}$ -ATPase in green (except for I829 and E255). The nets represent the omit-annealed  $F_0 - F_c$  map for TG (at 3 $\sigma$ , violet) and the water-accessible surface of  $\text{Ca}^{2+}$ -ATPase (green). The dashed pale-pink line shows a potential hydrogen bond between O8 of TG and NH of I829. The orientation of TG is consistent with the differences in affinity observed with natural variants and derivatives<sup>44</sup>.

between the A domain and M3 results in complete inhibition of the ATPase activity<sup>30,31</sup>, suggesting that the rotation of the A domain is another main event in the active transport by this pump. □

**Methods**

**Crystallization**

Affinity-purified enzyme<sup>32,33</sup> (20  $\mu\text{M}$ ) in detergent octaethyleneglycol mono-*n*-dodecylether ( $\text{C}_{12}\text{E}_8$ , 2 mg  $\text{ml}^{-1}$ ) and in 1 mM  $\text{Ca}^{2+}$  was mixed with thapsigargin (30  $\mu\text{M}$ ) and 3 mM EGTA, then dialysed against a buffer consisting of 2.75 M glycerol, 4% polyethylene glycol (PEG 400), 3 mM  $\text{MgCl}_2$ , 2.5 mM  $\text{NaN}_3$ , 2  $\mu\text{g ml}^{-1}$  butylhydroxytoluene, 0.2 mM dithiothreitol, 0.1 mM EGTA, 20 mM MES buffer at pH 6.1, for about 1 month. Crystals were grown to 200  $\times$  200  $\times$  50  $\mu\text{m}$  and flash-frozen in cold nitrogen gas.

**Data collection**

Diffraction data were collected at BL44XU, SPring-8, using a DIP2040 imaging plate detector (4,000  $\times$  4,000 pixels; MAC Science) at  $\lambda = 0.90 \text{ \AA}$ , and processed with Denzo and Scalepack<sup>34</sup>. Data from two of the best crystals were merged ( $R_{\text{merge}} = 9.2\%$  with a redundancy of 7.1 and  $I/\sigma = 21.2$ ) for 1/15.0 to 1/3.1  $\text{\AA}^{-1}$  (43.7%, 4.1, 3.0, respectively, for the highest resolution bin, 3.18–3.10  $\text{\AA}$ ). The crystals belonged to space group  $P4_1$  (unit cell dimensions of  $a = b = 71.7 \text{ \AA}$  and  $c = 590.3 \text{ \AA}$ ) and contained two protein molecules in the asymmetric unit.

**Modelling and refinement**

The modelling was started from a model<sup>10</sup> for the cytoplasmic part of the enzyme in the tubular crystals<sup>12</sup>. Initial refinement<sup>35</sup> was done with the N and P domains, then the A domain was included. The rest of the structure was gradually constructed by many iterations of map drawing, solvent flattening with Solomon<sup>36</sup> and model building using Turbo-Prodo (BioGraphics). The model, consisting of 7,717 atoms (7,673 in the protein, 44 in thapsigargin), was refined with CNS<sup>37</sup> using 50,822 reflections (at 95.7% completeness) to an  $R_{\text{free}}$  of 0.268 ( $R_{\text{cryst}} = 0.237$ ); r.m.s. bond length and angle were 0.009  $\text{\AA}$  and 1.3 $^\circ$ , respectively. Strict non-crystallographic symmetry constraints were applied throughout. The geometry of the model was examined with Procheck<sup>36</sup> and no residues (except for Gly) had dihedral angles in the disallowed region. The secondary structures were assigned with DSSP<sup>38</sup>. Crystal structures of trilobolide<sup>39</sup> and an epoxide of thapsigargin<sup>40</sup> were used as the initial model of thapsigargin.

Received 4 April; accepted 27 June 2002; doi:10.1038/nature00944.

1. Møller, J. V., Juul, B. & le Maire, M. Structural organization, ion transport, and energy transduction of P-type ATPases. *Biochim. Biophys. Acta* **1286**, 1–51 (1996).
2. MacLennan, D. H., Rice, W. J. & Green, N. M. The mechanism of  $\text{Ca}^{2+}$  transport by sarco(endo)plasmic reticulum  $\text{Ca}^{2+}$ -ATPases. *J. Biol. Chem.* **272**, 28815–28818 (1997).
3. Lee, A. G. & East, J. M. What the structure of a calcium pump tells us about its mechanism. *Biochem. J.* **356**, 665–683 (2001).
4. Yu, X., Carroll, S., Rigaud, J. L. & Inesi, G.  $\text{H}^+$  countertransport and electrogenicity of the

- sarcolemmal  $\text{Ca}^{2+}$  pump in reconstituted proteoliposomes. *Biophys. J.* **64**, 1232–1242 (1993).
5. Post, R. L., Hegyvary, C. & Kume, S. Activation by adenosine triphosphate in the phosphorylation kinetics of sodium and potassium ion transport adenosine triphosphatase. *J. Biol. Chem.* **247**, 6530–6540 (1972).
6. Albers, R. W. Biochemical aspects of active transport. *Annu. Rev. Biochem.* **36**, 727–756 (1967).
7. de Meis, L. & Vianna, A. L. Energy interconversion by the  $\text{Ca}^{2+}$ -dependent ATPase of the sarcoplasmic reticulum. *Annu. Rev. Biochem.* **48**, 275–292 (1979).
8. Aravind, L., Galperin, M. Y. & Koonin, E. V. The catalytic domain of the P-type ATPase has the haloacid dehalogenase fold. *Trends Biochem. Sci.* **23**, 127–129 (1998).
9. Johnson, L. N. & Lewis, R. J. Structural basis for control by phosphorylation. *Chem. Rev.* **101**, 2209–2242 (2001).
10. Toyoshima, C., Nakasako, M., Nomura, H. & Ogawa, H. Crystal structure of the calcium pump of sarcoplasmic reticulum at 2.6  $\text{\AA}$  resolution. *Nature* **405**, 647–655 (2000).
11. Xu, C., Rice, W. J., He, W. & Stokes, D. L. A structural model for the catalytic cycle of  $\text{Ca}^{2+}$ -ATPase. *J. Mol. Biol.* **316**, 201–211 (2002).
12. Zhang, P., Toyoshima, C., Yonekura, K., Green, N. M. & Stokes, D. L. Structure of the calcium pump from sarcoplasmic reticulum at 8- $\text{\AA}$  resolution. *Nature* **392**, 835–839 (1998).
13. Danko, S. *et al.* ADP-insensitive phosphoenzyme intermediate of sarcoplasmic reticulum  $\text{Ca}^{2+}$ -ATPase has a compact conformation resistant to proteinase K, V8 protease and trypsin. *FEBS Lett.* **489**, 277–282 (2001).
14. Danko, S., Yamasaki, K., Daiho, T., Suzuki, H. & Toyoshima, C. Organization of cytoplasmic domains of sarcoplasmic reticulum  $\text{Ca}^{2+}$ -ATPase in  $\text{E}_1\text{P}$  and  $\text{E}_1\text{ATP}$  states: a limited proteolysis study. *FEBS Lett.* **505**, 129–135 (2001).
15. Sagara, Y. & Inesi, G. Inhibition of the sarcoplasmic reticulum  $\text{Ca}^{2+}$  transport ATPase by thapsigargin at subnanomolar concentrations. *J. Biol. Chem.* **266**, 13503–13506 (1991).
16. Hayward, S. Structural principles governing domain motions in proteins. *Proteins* **36**, 425–435 (1999).
17. Zhang, Z., Lewis, D., Sumbilla, C., Inesi, G. & Toyoshima, C. The role of the M6-M7 loop (L67) in stabilization of the phosphorylation and  $\text{Ca}^{2+}$  binding domains of the sarcoplasmic reticulum  $\text{Ca}^{2+}$ -ATPase (SERCA). *J. Biol. Chem.* **276**, 15232–15239 (2001).
18. Zhang, Z. *et al.* Mutational analysis of the peptide segment linking phosphorylation and  $\text{Ca}^{2+}$ -binding domains in the sarcoplasmic reticulum  $\text{Ca}^{2+}$ -ATPase. *J. Biol. Chem.* **270**, 16283–16290 (1995).
19. Andersen, J. P., Vilsen, B. & MacLennan, D. H. Functional consequences of alterations to Gly310, Gly770, and Gly801 located in the transmembrane domain of the  $\text{Ca}^{2+}$ -ATPase of sarcoplasmic reticulum. *J. Biol. Chem.* **267**, 2767–2774 (1992).
20. Zhang, Z. *et al.* Detailed characterization of the cooperative mechanism of  $\text{Ca}^{2+}$  binding and catalytic activation in the  $\text{Ca}^{2+}$  transport (SERCA) ATPase. *Biochemistry* **39**, 8758–8767 (2000).
21. Andersen, J. P. & Vilsen, B. Amino acids Asn796 and Thr799 of the  $\text{Ca}^{2+}$ -ATPase of sarcoplasmic reticulum bind  $\text{Ca}^{2+}$  at different sites. *J. Biol. Chem.* **269**, 15931–15936 (1994).
22. Glusker, J. P. Structural aspects of metal liganding to functional groups in proteins. *Adv. Protein Chem.* **42**, 1–76 (1991).
23. Medda, P., Fassold, E. & Hasselbach, W. The effect of monovalent and divalent cations on the ATP-dependent  $\text{Ca}^{2+}$ -binding and phosphorylation during the reaction cycle of the sarcoplasmic reticulum  $\text{Ca}^{2+}$ -transport ATPase. *Eur. J. Biochem.* **165**, 251–259 (1987).
24. Yu, M. *et al.* Specific substitutions at amino acid 256 of the sarcoplasmic/endoplasmic reticulum  $\text{Ca}^{2+}$  transport ATPase mediate resistance to thapsigargin in thapsigargin-resistant hamster cells. *J. Biol. Chem.* **273**, 3542–3546 (1998).
25. Hua, S. & Inesi, G. Synthesis of a radioactive azido derivative of thapsigargin and photolabeling of the sarcoplasmic reticulum ATPase. *Biochemistry* **36**, 11865–11872 (1997).
26. Pikula, S., Mullner, N., Dux, L. & Martonosi, A. Stabilization and crystallization of  $\text{Ca}^{2+}$ -ATPase in detergent-solubilized sarcoplasmic reticulum. *J. Biol. Chem.* **263**, 5277–5286 (1988).
27. Juul, B. *et al.* Do transmembrane segments in proteolyzed sarcoplasmic reticulum  $\text{Ca}^{2+}$ -ATPase retain their functional  $\text{Ca}^{2+}$  binding properties after removal of cytoplasmic fragments by proteinase K? *J. Biol. Chem.* **270**, 20123–20134 (1995).
28. Lutsenko, S., Anderko, R. & Kaplan, J. H. Membrane disposition of the M5-M6 hairpin of  $\text{Na}^+$ ,  $\text{K}^+$ -ATPase  $\alpha$  subunit is ligand dependent. *Proc. Natl Acad. Sci. USA* **92**, 7936–7940 (1995).
29. Gatto, C., Lutsenko, S., Shin, J. M., Sachs, G. & Kaplan, J. H. Stabilization of the H,K-ATPase M5M6 membrane hairpin by  $\text{K}^+$  ions. Mechanistic significance for P2-type ATPases. *J. Biol. Chem.* **274**, 13737–13740 (1999).
30. Juul, B. & Møller, J. V. In *Na/K-ATPase and Related ATPases* (eds Taniguchi, K. & Kaya, S.) 233–236 (Elsevier, Amsterdam, 2000).
31. Jørgensen, P. L. & Collins, J. H. Tryptic and chymotryptic cleavage sites in sequence of  $\alpha$ -subunit of ( $\text{Na}^+ + \text{K}^+$ )-ATPase from outer medulla of mammalian kidney. *Biochim. Biophys. Acta* **860**, 570–576 (1986).
32. Coll, R. J. & Murphy, A. J. Purification of the CaATPase of sarcoplasmic reticulum by affinity chromatography. *J. Biol. Chem.* **259**, 14249–14254 (1984).
33. Stokes, D. L. & Green, N. M. Three-dimensional crystals of CaATPase from sarcoplasmic reticulum. Symmetry and molecular packing. *Biophys. J.* **57**, 1–14 (1990).
34. Otwinowski, Z. & Minor, W. Processing of X-ray diffraction data collected in oscillation mode. *Methods Enzymol.* **276**, 307–325 (1997).
35. Brünger, A. T. Extension of molecular replacement: a new search strategy based on Patterson correlation refinement. *Acta Crystallogr. A* **46**, 46–57 (1990).
36. Collaborative Computational Project No. 4 The CCP4 suite: programs for protein crystallography. *Acta Crystallogr. D* **50**, 760–763 (1994).
37. Brünger, A. T. *et al.* Crystallography & NMR system: A new software suite for macromolecular structure determination. *Acta Crystallogr. D* **54**, 905–921 (1998).
38. Kabsch, W. & Sander, C. Dictionary of protein secondary structure: pattern recognition of hydrogen-bonded and geometrical features. *Biopolymers* **22**, 2577–2637 (1983).
39. Kutschabsky, L., Kretschmer, R.-G. & Ripperger, H. The crystal and molecular structure of the sesquiterpenoid silerin (trilobolide). *Crystal Res. Technol.* **21**, 627–633 (1986).
40. Christensen, S. B., Larsen, I. K., Rasmussen, U. & Christopherson, C. Thapsigargin and thapsigarginin, two histamine liberating sesquiterpene lactones from *Thapsia garganica*. X-ray analysis of the 7,11-epoxide of thapsigargin. *J. Org. Chem.* **47**, 649–652 (1982).

41. MacLennan, D. H., Brandl, C. J., Korczak, B. & Green, N. M. Amino-acid sequence of a  $\text{Ca}^{2+}$  +  $\text{Mg}^{2+}$ -dependent ATPase from rabbit muscle sarcoplasmic reticulum, deduced from its complementary DNA sequence. *Nature* **316**, 696–700 (1985).
42. James, P., Inui, M., Tada, M., Chiesi, M. & Carafoli, E. Nature and site of phospholamban regulation of the  $\text{Ca}^{2+}$  pump of sarcoplasmic reticulum. *Nature* **342**, 90–92 (1989).
43. Kraulis, P. J. MOLSCRIPT: a program to produce both detailed and schematic plots of protein structures. *J. Appl. Crystallogr.* **24**, 946–950 (1991).
44. Christensen, S. B., Andersen, A. & Smitt, U. W. Sesquiterpenoids from *Thapsia* species and medicinal chemistry of the thapsigargin. *Fort. Chem. Org. Nat.* **71**, 129–167 (1997).

Supplementary Information is available on Nature's website (<http://www.nature.com/nature>).

### Acknowledgements

We thank H. Ogawa for help in data gathering, R. Yoshida for computations, and M. Nakasako for modelling. We also thank G. Inesi, P. Champeil, D. B. McIntosh and

H. Suzuki for communicating unpublished results to us and for their help in improving the manuscript. Thanks are also due to E. Yamashita and all the staff at BL44XU of SPring-8. This work was supported in part by Grants-in-Aid for Scientific Research from the Ministry of Education, Culture, Sports, Science and Technology, the Japan New Energy and Industry Technology Development Organization, and the Human Frontier Science Program.

### Competing interests statement

The authors declare that they have no competing financial interests.

Correspondence and requests for materials should be addressed to C.T. (e-mail: [ct@iam.u-tokyo.ac.jp](mailto:ct@iam.u-tokyo.ac.jp)). The atomic coordinates are deposited in the PDB (accession code 1IWO).